Quantum cutting in Li (770 nm) and Yb (1000 nm) co-dopant emission bands by energy transfer from the ZnO nano-crystalline host

M. V. Shestakov,[1,2] V. K. Tikhomirov,[1,*] D. Kirilenko,[3] A. S. Kuznetsov,[1] L. F. Chibotaru,[4] A. N. Baranov,[5] G. Van Tendeloo,[3] V. V. Moshchalkov[1]

[1] *INPAC – Institute for Nanoscale Physics and Chemistry, Katholieke Universiteit Leuven, Belgium*
[2] *Department of Materials Science, Lomonosov Moscow State University, Moscow, Russia*
[3] *EMAT, Electron Microscopy for Materials Science, Universiteit Antwerpen, Belgium*
[4] *Department of Chemistry, Katholieke Universiteit Leuven, Belgium*
[5] *Department of Chemistry, Lomonosov Moscow State University, Moscow, Russia*
[*] *Victor.Tikhomirov@fys.kuleuven.be*

Abstract: Li-Yb co-doped nano-crystalline ZnO has been synthesized by a method of thermal growth from the salt mixtures. X-ray diffraction, transmission electron microscopy, atomic absorption spectroscopy and optical spectroscopy confirm the doping and indicate that the dopants may form Li-Li and Yb^{3+}-Li based nanoclusters. When pumped into the conduction and exciton absorption bands of ZnO between 250 to 425 nm, broad emission bands of about 100 nm half-height-width are excited around 770 and 1000 nm, due to Li and Yb dopants, respectively. These emission bands are activated by energy transfer from the ZnO host mostly by quantum cutting processes, which generate pairs of quanta in Li (770 nm) and Yb (1000 nm) emission bands, respectively, out of one quantum absorbed by the ZnO host. These quantum cutting phenomena have great potential for application in the down-conversion layers coupled to the Si solar cells.

OCIS codes: (160.4236) Nanomaterials; (250.5230) Photoluminescence; (160.6000) Semiconductor materials.

References and links

1. W. Shockley and H. J. Queisser, "Detailed balance limit of efficiency of p-n junction solar cells," J. Appl. Phys. **32**(3), 510–518 (1961).
2. B. Richards, "Enhancing the performance of silicon solar cells via the application of passive luminescence conversion layers," Sol. Energy Mater. Sol. Cells **90**(15), 2329–2337 (2006).
3. T. Trupke, A. Shalav, B. S. Richards, P. W. Würfel, and M. A. Green, "Efficiency enhancement of solar cells by luminescent up-conversion of sun light," Sol. Energy Mater. Sol. Cells **90**(18-19), 3327–3338 (2006).
4. J. de Wild, J. K. Rath, A. Meijerink, W. Van Sark, and R. E. I. Schropp, "Enhanced near-infrared response of a-Si:H solar cells with β-$NaYF_4$:Yb^{3+} (18%), Er^{3+} (2%) up-conversion phosphors," Sol. Energy Mater. Sol. Cells **94**(12), 2395–2398 (2010).
5. V. D. Rodríguez, V. K. Tikhomirov, J. Méndez-Ramos, J. del-Castillo, and C. Görller-Walrand, "Measurement of quantum yield of up-conversion Luminescence in $Er^{(3+)}$-doped nano-glass-ceramics," J. Nanosci. Nanotechnol. **9**(3), 2072–2075 (2009).
6. J. Méndez-Ramos, V. K. Tikhomirov, V. D. Rodríguez, and D. Furniss, "Infrared tunable up-conversion phosphor based on Er^{3+} doped nano-glass-ceramics," J. Alloy. Comp. **440**(1-2), 328–332 (2007).
7. T. Fukuda, S. Kato, E. Kin, K. Okaniwa, H. Morikawa, Z. Honda, and N. Kamata, "Wavelength conversion film with glass coated Eu chelate for enhanced silicon-photovoltaic cell performance," Opt. Mater. **32**(1), 22–25 (2009).
8. B. M. van der Ende, L. Aarts, and A. Meijerink, "Near-infrared quantum cutting for photovoltaics," Adv. Mater. (Deerfield Beach Fla.) **21**(30), 3073 (2009).
9. V. D. Rodríquez, V. K. Tikhomirov, J. Méndez-Ramos, A. C. Yanes, and V. V. Moshchalkov, "Towards broad range and highly efficient down-conversion of solar spectrum by Er^{3+}-Yb^{3+} co-doped nano-structured glass-ceramics," Sol. Energy Mater. Sol. Cells **94**(10), 1612–1617 (2010).
10. V. K. Tikhomirov, V. D. Rodríguez, A. Kuznetsov, D. Kirilenko, G. Van Tendeloo, and V. V. Moshchalkov, "Preparation and luminescence of bulk oxyfluoride glasses doped with Ag nanoclusters," Opt. Express **18**(21), 22032–22040 (2010).

#149477 - $15.00 USD Received 17 Jun 2011; revised 11 Jul 2011; accepted 19 Jul 2011; published 4 Aug 2011

11. S. Ye, N. Jiang, F. He, X. Liu, B. Zhu, Y. Teng, and J. R. Qiu, "Intense near-infrared emission from ZnO-$LiYbO_{(2)}$ hybrid phosphors through efficient energy transfer from ZnO to $Yb^{(3+)}$," Opt. Express **18**(2), 639–644 (2010).
12. Y. Teng, J. Zhou, X. Liu, S. Ye, and J. Qiu, "Efficient broadband near-infrared quantum cutting for solar cells," Opt. Express **18**(9), 9671–9676 (2010).
13. A. Klein, B. Rech, and K. Ellme, *Transparent Conductive Zinc Oxide*, eds. (Springer, Berlin, 2008).
14. C. Klingshirn, "ZnO: From basics towards applications," Phys. Status Solidi, B Basic Res. **244**(9), 3027–3073 (2007).
15. Ü. Özgür, Y. I. Alivov, C. Liu, A. Teke, M. A. Reshchikov, S. Doğan, V. Avrutin, S.-J. Cho, and H. Morkoç, "A comprehensive review of ZnO materials and devices," J. Appl. Phys. **98**(4), 041301 (2005).
16. A. van Dijken, E. A. Meulenkamp, D. Vanmaekelbergh, and A. Meijerink, "The luminescence of nanocrystalline ZnO particles: the mechanism of the ultraviolet and visible emission," J. Lumin. **87–89**, 454–456 (2000).
17. Z. Zhou, T. Komori, T. Ayukawa, H. Yukawa, M. Morinaga, A. Koizumi, and Y. Takeda, "Li- and Er-codoped ZnO with enhanced 1.54 μm photoemission," Appl. Phys. Lett. **87**(9), 091109 (2005).
18. T. Fan, Q. Zhang, and Z. Jiang, "Enhanced near-infrared luminescence in Y_2O_3:Yb^{3+} nanocrystals by codoping with Li^+ ions," Opt. Commun. **284**(1), 249–251 (2011).
19. A. N. Baranov, G. N. Panin, T. W. Kang, and Y.-J. Oh, "Growth of ZnO nanorods from a salt mixture," Nanotechnology **16**(9), 1918–1923 (2005).
20. A. N. Baranov, C. H. Chang, O. A. Shlyakhtin, G. N. Panin, T. W. Kang, and Y.-J. Oh, "In situ study of the ZnO–NaCl system during the growth of ZnO nanorods," Nanotechnology **15**(11), 1613–1619 (2004).
21. I. Sakaguchi, Y. Adachi, T. Ogaki, K. Matsumoto, S. Hishita, H. Haneda, and N. Ohashi, "Impurity contamination and diffusion during annealing in implanted ZnO," Key Eng. Mater. **388**, 23–26 (2009).
22. Y. Hashimoto, M. Wakeshima, K. Matsuhira, Y. Hinatsu, and Y. Ishii, "Structures and magnetic properties of ternary lithium oxides $LiRO_2$ (R=Rare Earths)," Chem. Mater. **14**(8), 3245–3251 (2002).
23. R. E. LaVilla, "$M_{4,5}$ emission spectra from Gd_2O_3 and Yb_2O_3," Phys. Rev. A **9**(5), 1801–1805 (1974).
24. C. Dallera, E. Annese, J.-P. Rueff, A. Palenzona, G. Vanko, L. Braicovich, A. Shukla, and M. Grioni, "Determination of pressure-induced valence changes in $YbAl_2$ by resonant inelastic X-ray emission," Phys. Rev. B **68**(24), 245114 (2003).
25. Y. Ding and Z. L. Wang, "Electron energy-loss spectroscopy study of ZnO nanobelts," J. Electron Microsc. (Tokyo) **54**(3), 287–291 (2005).
26. N. R. Yogomalar and A. C. Bose, "Burnstein-Moss shift and room temperature near-band-edge luminescence in lithium doped zinc oxide," Appl. Phys., A Mater. Sci. Process. **103**(1), 33–42 (2011).
27. V. K. Tikhomirov, K. Driesen, C. Görller-Walrand, and M. Mortier, "Broadband telecommunication wavelength emission in Yb^{3+}-Er^{3+}-Tm^{3+} co-doped nano-glassceramics," Opt. Express **15**(15), 9535–9540 (2007).
28. E. L. Nicholas and H. L. Howes, "The photolumenscence of flames," Phys. Rev. **22**(5), 425–431 (1923).
29. L. J. Radziemski, R. Engleman, Jr., and J. W. Brault, "Fourier-transform-spectroscopy measurements in the spectra of neutral lithium, 6Li," Phys. Rev. A **52**(6), 4462–4470 (1995).
30. A. Carvahlo, A. Alakauskas, A. Pasquarello, A. K. Tagantsev, and N. Setter, "Li-related defects in ZnO: Hybrid functional calculations," Physica B **404**(23-24), 4797–4799 (2009).
31. A. N. Alexandrova, A. I. Boldyrev, X. Li, H. W. Sarkas, J. H. Hendricks, S. T. Arnold, and K. H. Bowen, "Lithium cluster anions: photoelectron spectroscopy and ab initio calculations," J. Chem. Phys. **134**(4), 044322 (2011).
32. T. Hirai, Y. Harada, S. Hashimoto, T. Itoh, and N. Ohno, "Luminescence of excitons in mesoscopic ZnO particles," J. Lumin. **112**(1-4), 196–199 (2005).
33. G. Alombert-Godet, C. Armellini, S. Berneschi, A. Chiappini, A. Chiasera, M. Ferrari, S. Guddala, E. Moser, S. Pelli, D. N. Rao, and G. C. Righini, "Tb^{3+}/Yb^{3+} co-activated silica-hafnia glass ceramic waveguides," Opt. Mater. **33**(2), 227–230 (2010).

1. Introduction

According to the Shockley-Queisser criterion, the theoretical maximum efficiency of silicon solar cells cannot exceed 30% [1,2]. The up-conversion [3–6 and refs therein] and down-conversion [7–12 and refs therein] layers applied to the back and front surfaces of the solar cells, respectively, have been proposed for overcoming the above criterion, potentially resulting in the enhanced efficiency of the solar cells. The down-conversion of solar spectrum looks especially promising as it does not require high power density for solar radiation and thus avoids the use of the solar light concentrators.

In the down-conversion process, the absorbed photons from the range about 300 to 500 nm generate the photons with lower energy in the range 550 to 1100 nm with a quantum yield approaching 100% for conventional phosphors [2,7] or even 200% for quantum cutting processes [8,9,11,12 and refs therein]. In this respect, the down-conversion layers codoped with Yb^{3+} ion attract particular interest because Yb^{3+} has a unique emission band about 1000 nm with high emission cross-section, which falls in the spectral range where light-to-current

#149477 - $15.00 USD Received 17 Jun 2011; revised 11 Jul 2011; accepted 19 Jul 2011; published 4 Aug 2011

energy conversion efficiency (ECE) of Si solar cells reaches a maximum of 100% [2,8–12 and refs therein].

Zinc oxide (ZnO) doped with Yb^{3+} has been proposed for broad-band high quantum yield down-conversion of solar spectrum by energy transfer from ZnO absorber to Yb^{3+} emitter [11 and refs therein]. ZnO has several advantages with respect to down-conversion: it is a direct wide gap semiconductor with high absorption cross-section in the wavelength range of 250 to 450 nm (band-band and exciton absorption transitions) and high transparency in the visible and near infrared ranges, e.g. in [13–16]. Al-doped ZnO can also be used as a transparent front electrode in solar cells, and ZnO nanorods may be used as an active medium in solar cells with enhanced area of p-n transition, e.g. in [13]. Combining the above mentioned properties of ZnO can be of obvious benefit for enhancement of the efficiency of the solar cells.

The Li is known to increase luminescence efficiency of rare-earth co-dopants, e.g. in [17,18], and the ZnO-$LiYbO_2$ composite was proposed for efficient energy transfer from ZnO to Yb^{3+} [11].

Here we report on preparation of ZnO nanopowder co-doped with Li and Yb, presumably in the structure of Li-Li and Yb^{3+}-Li based nanoclusters. We have observed unusual luminescence band ascribed to the neutral Li-Li nanoclusters in the near infrared range around 770 nm by energy transfer/quantum cutting from the ZnO host under excitation in a broad absorption band of ZnO between 250 to 450 nm, corresponding to the band-band and exciton absorption transitions in ZnO. In addition, the emission band of Yb has been also excited at about 1000 nm by energy transfer/quantum cutting from ZnO. Pump power dependence and temperature dependence of these luminescence bands indicate that mostly the quantum cutting mechanisms are involved in energy transfer from ZnO to Li and Yb dopants. The mechanisms for the above energy transfers and for the excitation of Li and Yb emission bands have been suggested.

2. Experimental

We have used the method for preparation of the ZnO nanopowders doped with Li as it was described elsewhere [19,20]; whilst in this work we have also added in some cases an Yb-containing precursor. Hence, the $Zn(NO_3)_2$ and $Yb(NO_3)_3$ aqueous solutions have been prepared, mixed and precipitated by excessive amount of another aqueous NH_4HCO_3 solution. The $Yb(NO_3)_3$ concentration was varied from 0 to 1.0 mol% to get samples with different Yb doping levels. The precipitated zinc carbonate hydroxide containing Yb dopant (ZCH) was washed by distilled water and freeze dried. Further, a salt mixture was prepared with a ratio of 0.5 g ZCH/ 9g NaCl/ 1g Li_2CO_3., while the proportion of Li_2CO_3 was varied from 0 to 10 wt% to get samples with different Li doping level. The mixtures have been sintered at 700°C for 2 h, and the products were washed again to remove residuals of NaCl. The resulting nanopowders have been pressed into pellets either as prepared or with an added KBr powder.

The effect of extra heat-treatment has been investigated when heat-treating the samples at 600°C, especially to initiate the diffusion of Li ions. A heat-treatment at this temperature ensures a high diffusion coefficient of Li in ZnO [21].

The photoluminescence (PL) spectra have been measured with CCD cameras Andor Technologies iXon DV887 FL (500 to 1100 nm range) and Prinston Instruments OMA V (650 to 1700 nm range), and with a conventional spectrometer Edinburgh Instruments FS920 equipped with an extended Hamamatsu photomultiplier (200 to 1100 nm range). In the latter case, the excitation spectra of luminescence have been also measured. The spectral response of the setups was taken into account. The pump power dependence of luminescence has been measured when pumped by Ar laser operated at 355 nm and 2 mW; the pump power was varied by about 100 times with calibrated neutral filters. The temperature dependence of luminescence has been measured from the room temperature down to 10 K when placing the sample pellet in a helium flow cryostat.

Transmission electron microscopy (TEM) measurements have been carried out using a Jeol JEM-3000F microscope equipped with an energy dispersion X-ray spectrometer (EDX).

#149477 - $15.00 USD Received 17 Jun 2011; revised 11 Jul 2011; accepted 19 Jul 2011; published 4 Aug 2011

Specimens were prepared by grinding the sample powder in methanol and casting a drop of the obtained suspension on a lacey carbon film. The Yb-content in the samples has been extracted from the TEM EDX spectra.

The Li-content in the samples has been estimated by atomic absorption spectroscopy (AAS) using the Perkin-Elmer AAS-303 spectrometer, and from X-ray diffraction (XRD) measurements using the RIGAKU diffractometer.

3. Results

3.1 XRD, TEM EDX and ASS studies

The X-ray diffraction patterns of the samples of interest are shown in Fig. 1. The samples presented in Fig. 1 will be called further in the text as ZnO, ZnO:Li and ZnO:Li-Yb samples, respectively, and the further shown experimental data have been obtained on these samples. All diffraction peaks of the ZnO (black curve) and ZnO:Li (red curve) nanopowders are identified as wurtzite ZnO peaks (JCPDC card 36-1451). The ZnO:Li-Yb nanopowder (blue curve) shows additionally, as indicated by the stars and down-headed arrows, minor admixtures of the Yb_2O_3 (JCPDC card 41-1106) and $LiYbO_2$ crystalline phases, respectively. The diffraction peaks corresponding to the $LiYbO_2$ phase are identified in agreement with Ref [22]; most of these peaks are very weak and are not visible on the scale of Fig. 1.

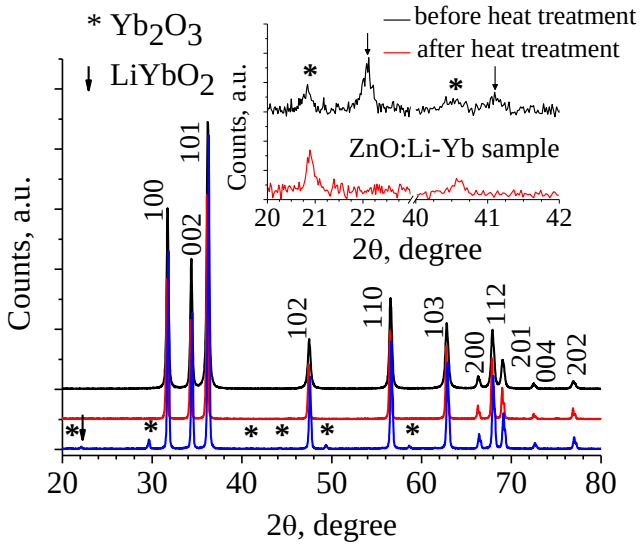

Fig. 1. XRD pattern taken from nanopowders of ZnO (black curve), ZnO:Li (red curve) and ZnO:Li-Yb (blue curve). Insert shows zoomed areas for ZnO:Li-Yb nanopowder before and after heat-treatment at 600°C for 30 minutes. Miller indices indicate the crystalline planes of ZnO wurtzite structure. The diffraction peaks corresponding to the Yb_2O_3 and $LiYbO_2$ crystalline phases are marked by star * and down-headed arrow ↓ respectively. CuKα X-ray line was used.

The insert in Fig. 1 depicts the effect of heat-treatment on the XRD pattern of the ZnO:Li-Yb nanopowder: the $LiYbO_2$ phase vanishes after this heat-treatment. However, we shall see further that this heat-treatment does not quenches emission band of Li pointing out that the $LiYbO_2$ phase is not the only pre-requisite for the observed Li luminescence. The fact that the $LiYbO_2$ and Yb_2O_3 phases can be detected in XRD patterns in Fig. 1 indicates that Li and Yb atoms comprise an amount of the order of 1 at% each in the ZnO:Li-Yb sample; this will be confirmed further in the text.

#149477 - $15.00 USD Received 17 Jun 2011; revised 11 Jul 2011; accepted 19 Jul 2011; published 4 Aug 2011

The chemical composition of the samples has also been investigated by means of TEM EDX and AAS. Figure 2(a) presents a low magnification TEM image of the ZnO:Li-Yb sample; the nanopowder consists of grains in the range 50 to 500 nm. TEM EDX data, Fig. 2(b); indicate that Yb is present in the sample and that the detected concentration of Yb is about 1 at%. Of special interest are the $M_{4,5}$ peaks of Yb between 1.50 to 2.00 keV; they are zoomed in the insert to Fig. 2(b), and identified by the software of the EDX spectrometer. The ratio of these peaks is unusual for a Yb^{3+} valence state of Yb ions (see for example in [23,24]). For an Yb^{3+} valence, the low energy peak at 1.50 keV dominates over the high energy peak at 1.70 keV, while in Fig. 2(b) the 1.70 keV peak dominates over the 1.50 keV peak. This unusual ratio may indicate that the surrounding and the valence state of the Yb dopant may vary from site to site in the regular ZnO crystalline host; this is most probably related to the presence of Li impurity ions attached to or nearby the Yb^{3+} ions. A fluctuation of the valence state of Yb between + 3 and + 2 is typical for the Yb dopant in a variety of hosts (e.g. in [12 and refs therein]). Thus, Yb^{3+}-Li dimers/nanoclusters may possibly be formed in the ZnO:Li-Yb samples, resulting in a minor change of the outer shell electron structure and the valence of the Yb ions.

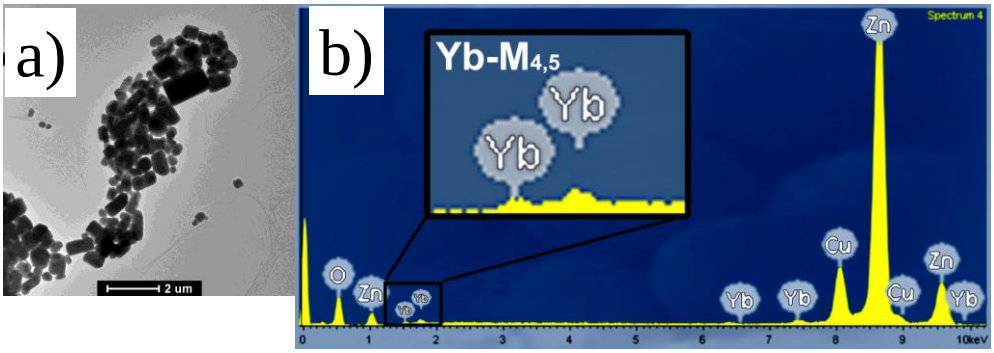

Fig. 2. (a) TEM image and (b) TEM EDX spectrum of ZnO:Li-Yb nanopowder. The Yb-$M_{4,5}$ peaks between 1.50 and 2.00 keV are indicated and zoomed. Other peaks corresponding to the Yb, Zn and O are also labeled. Cu and C peaks are due to the sample holder.

The Li-content of the samples cannot be identified from the TEM EDX spectrum because Li is a very light element. Li cannot be detected either in the electron energy loss spectrum (EELS) of ZnO:Li and ZnO:Li-Yb samples because the third EELS harmonic of the ZnO host [25] occurs at the same value of 60 eV as the main inner-shell K-edge of Li and masks the EELS signal from Li. Therefore we applied the AAS technique and we found that the doping with Li was at about 1.5 at% for ZnO:Li as well as for ZnO:Li-Yb samples. This doping level of Li, together with 1 at% of Yb in the ZnO:Li-Yb sample, are high doping levels which therefore favor nanoclustering of Li-Li and Yb^{3+}-Li pairs.

3.2 Excitation and emission spectra of luminescence

Figure 3 shows photographs (a) and emission and excitation spectra of luminescence of samples ZnO (b), ZnO:Li (c) and ZnO:Li-Yb (d). Photographs in Fig. 3(a) show the luminescent spot seen on the surface of the ZnO:Li-Yb nanopowder pellet, when excited at 355 nm of Ar laser (invisible light), whilst the contour of the pellet itself can also be seen. An upper photograph was taken when the sample was exposed only to a beam of a laser, and a lower photograph was taken when the sample was additionally illuminated by an ambient light of a table lamp. The bright green-white luminescence has been visually observed in the former case and a bright white luminescence in the latter case, indicating that the sample emits a broad visible emission band covering the blue/green/red parts of the spectrum.

#149477 - $15.00 USD Received 17 Jun 2011; revised 11 Jul 2011; accepted 19 Jul 2011; published 4 Aug 2011

The excitation and the emission spectra of luminescence of undoped sample, Fig. 3(b), are typical of undoped ZnO crystals [14–16]; the photoexcited electrons travel in the conduction band until they are trapped by intrinsic defects in ZnO resulting in emission mostly in the green with some admixtures in the blue, yellow and red. The drop in excitation spectrum at about 380-400 nm corresponds to exciton absorption, which then results mostly in exciton luminescence in UV (not shown).

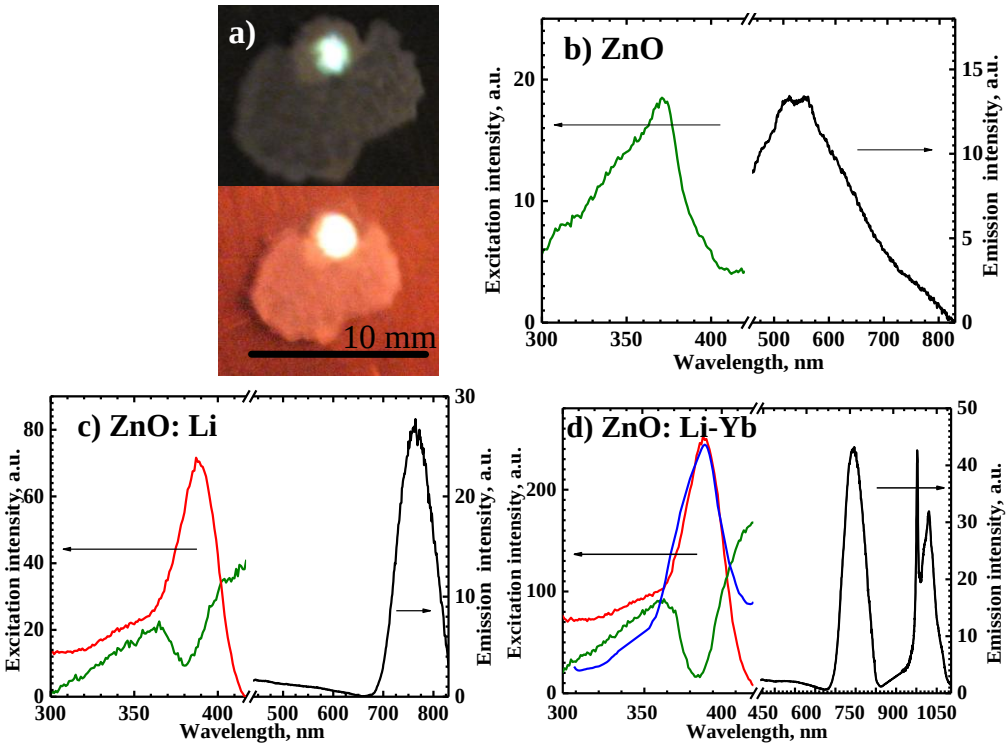

Fig. 3. (a) A piece of ZnO:Li-Yb nanopowder pellet showing a bright luminescent spot when illuminated by an invisible laser beam of Ar laser at 355 nm. (b,c,d) Excitation (left side) and emission (right side, black curves) spectra of ZnO (b), ZnO:Li (c) and ZnO:Li-Yb (d) nanopowders; in excitation spectra the green curves correspond to detection at 550 nm (intrinsic defect emission), red curves to detection at 770 nm (Li emission) and blue curve to detection at 980 nm (Yb emission).

Figure 3(c) shows that doping of ZnO with Li results in a new emission band in the near infrared about 770 nm, which is much stronger than the intrinsic emission bands of ZnO in the visible that define the luminescence color in Fig. 3(a). Thus, this band at 770 nm is due to Li dopants. Excitation spectrum of this band clearly corresponds to the absorption spectrum of ZnO with band-band transitions in the range 300 to 380 nm and exciton absorption transition around 380 nm [14–16]. This indicates that an energy transfer ZnO→Li takes place on excitation of the ZnO host. The maximum wavelength for excitation of the Li infrared band corresponds to the minimum wavelength for excitation of intrinsic green luminescence band of ZnO, indicating completely different mechanisms for their excitation. Noteworthy, a minimum in the green emission excitation curve shifts to the shorter wavelengths in this Li-doped sample compared to undoped sample, Fig. 3(b), indicating that Li incorporation increases a gap of ZnO, in agreement with data [26].

Figure 3(d) shows that co-doping with Li and Yb results in the same Li-related emission band at about 770 nm and another emission band at about 1000 nm, which is commonly associated with Yb^{3+} emission. The excitation spectra for these two bands are exactly the

#149477 - $15.00 USD Received 17 Jun 2011; revised 11 Jul 2011; accepted 19 Jul 2011; published 4 Aug 2011

same, indicating the similar mechanisms for their excitation by energy transfer from ZnO to Li and Yb. The mechanism for the transfer will be discussed further. Again the maxima for excitation of these bands correspond to the minimum of the excitation of intrinsic green luminescence. That is mostly the exciton state of ZnO, which transfers energy to Li and Yb related emission bands.

3.3 Effect of heat treatment in air on Li luminescence

We have undertaken heat treatment of ZnO:Li and ZnO:Li-Yb nanopowders at 600°C because it is known that the Li ions become mobile in ZnO crystalline network at this temperature [21]. Figure 4 demonstrates an effect of heat treatment in air atmosphere on the emission spectrum of ZnO:Li nanopowder: the Li-related band at 770 nm decreases and the green intrinsic luminescence band of ZnO at 550 nm shows a substantially weaker decrease. A decrease of green band intensity is readily understood, since it is known that ZnO picks up an oxygen when heat-treated in air and a number of its intrinsic defects decreases resulting in decrease of intrinsic green luminescence band of ZnO [14,15 and refs therein].

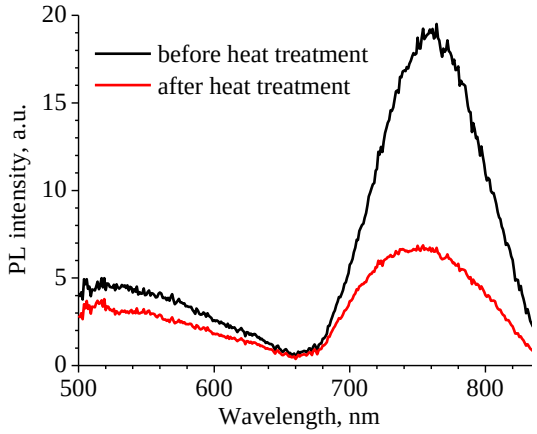

Fig. 4. Effect of heat treatment in air at 600°C for 30 minutes on emission spectrum of ZnO:Li nanopowder. Excitation was at 355 nm and 1 mW power of Ar laser.

On the other hand, a decrease in the intensity of Li-band may be due to a heat treatment induced condensation of Li ions into metallic Li droplets thus resulting in a decrease of the number of luminescent Li-Li nanoclusters. Li metal, as other metals, e.g. Ag [10], does not emit; thus accounting for the heat treatment induced decrease of Li luminescence.

3.4 Pump power and temperature dependence of Li luminescence

A pump power dependence of the luminescence intensity, I versus pump P, provides information about the mechanisms involved in the luminescence. For instance, in the case of up-conversion luminescence, the power equals to 2, i.e. the dependence is $I = P^2$, e.g [3–6], and in the case of down-conversion luminescence by a quantum cutting mechanism, the power equals to 0.5, i.e. the dependence is $I = P^{0.5}$, e.g. in [12]. Due to mismatch between the energies of the involved levels, phonon assistant or other cross-relaxation processes can be involved in the mechanism of luminescence resulting in lowering the power for the up-conversion luminescence to the values between 2 and 1, e.g. in [5], and increasing the power for the quantum cutting mechanism of luminescence to the values between 0.5 and 1.0 [12]. The slope of the Lg-Lg dependence of I versus P corresponds to the power; this dependence for the Li and Yb emission bands is shown in Fig. 5 for ZnO:Li (a) and ZnO:Li-Yb (b). The pump was done at 355 nm line of unfocused beam of Ar laser with decreasing the pump by two orders of magnitude from the value of 2 mW by calibrated neutral filters.

#149477 - $15.00 USD Received 17 Jun 2011; revised 11 Jul 2011; accepted 19 Jul 2011; published 4 Aug 2011

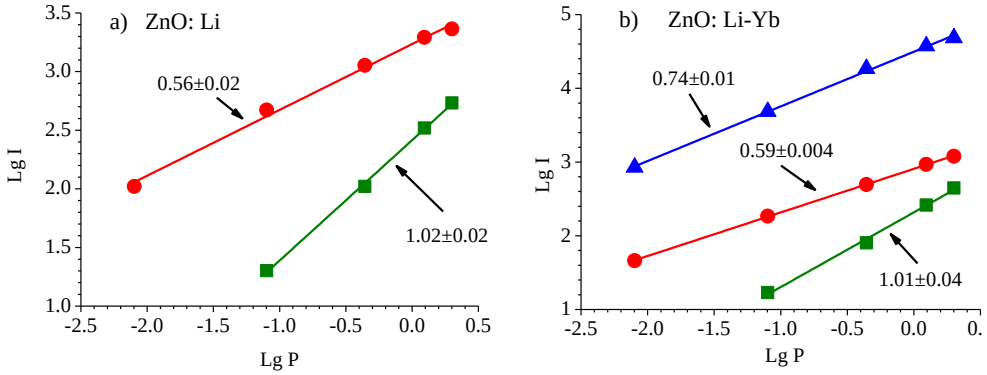

Fig. 5. Lg-Lg dependence of the emission intensity I versus the pump power P for the green 550 nm intrinsic emission band of ZnO (green color), for the 770 nm emission band of Li (red color) and for the 1000 nm emission band of Yb (blue color). The samples compositions and the slopes of the dependences are post-signed.

The power for the green emission band of ZnO, at 550 nm, is close to 1, which indicates normal dependence for one photon emission process. However, the power for Li band at 770 nm is close to 0.5 in both the ZnO:Li and the ZnO:Li-Yb samples, indicating that a quantum cutting process is involved in the Li emission, when one absorbed quantum by ZnO is converted into two emitted quanta in the Li-related emission band. The power for the Yb-related emission band is close to 0.75 indicating that both linear and quantum cutting processes are involved in the emission of the Yb-related band.

The temperature dependence of the luminescence reveals that the intrinsic green emission band in both the ZnO:Li and ZnO:Li-Yb samples increases monotonously with lowering the temperature down to 10 K. However, with lowering the temperature the Li and Yb-related emission bands vanish at about 150 K. This indicates a different mechanism for the excitation of the intrinsic emission band of ZnO (from the ZnO conduction band to the intrinsic defects in ZnO) and Li and Yb-related emission bands (excited mostly by energy transfer from the exciton band of ZnO). In the latter case, the dipole-dipole interaction amongst the Li-Li and Yb-Li pairs and ZnO exciton may be mediated/amplified by the host phonons, which become frozen by lowering the temperature, similar to the case of the energy transfer process between Er, Tm and Yb co-dopants in an oxyfluoride glass-ceramics host [27].

4. Discussion

Reports on the luminescence of Li are rather scarce. Li gas emits in the red at about 670 nm when heated in the flame, i.e. when excited by a multi-phonon absorption process [28]. The energy levels of Li atoms have been summarized in [29], where one can see that apparently only this red emission/absorption transition of Li at about 670 nm = 14900 cm^{-1} has a high oscillator strength, while other transitions of Li are orders of magnitude weaker. This may be a reason for the scarcity of data about Li luminescence. The excited energy level, doublet $^2P_{3/2}$,$^2P_{1/2}$, for this transition, for a single Li atom, is shown in the diagram of Fig. 6 as a horizontal thin red line.

The experimentally found emitting levels for Li dopants, as deduced from the data of Fig. 3c,d, are shown as thick horizontal red lines for a pair of the neighboring Li atoms in Fig. 6. The actual emitting levels of Li are substantially lower than those for the single Li atoms, and therefore we may conclude that Li atoms form a kind of nanocluster in our samples, presumably Li-Li dimers. This normally results in a red shift of the energy levels of the nanoclusters compared to single atoms, as e.g. in the case of Ag nanoclusters [10 and refs therein]. We rule out the charged Li^+-Li^+ and Li^+-Li dimers because the excited energy levels of Li^+ locate very high in the UV. The structure of the Li-Li dimers/nanoclusters, the origin of their dipole-dipole interaction with exciton state of the ZnO and the modeling their emission

#149477 - $15.00 USD Received 17 Jun 2011; revised 11 Jul 2011; accepted 19 Jul 2011; published 4 Aug 2011

spectra will be a topic for further extensive work and it is out of scope of this paper. Meanwhile, Li ions are known to agglomerate readily into nanoclusters due to the high ionic mobility of Li, e.g. in [30,31 and refs therein].

Li atoms locate next to each other in the Li-Li dimers/nanoclusters, this promotes a cooperative quantum cutting processes [8,9,11,12] as deduced from the data of Fig. 5a,b, and indicated by the dashed lines in Fig. 6. A decaying exciton can excite two Li atoms simultaneously/cooperatively only if they are *neighbors*, due to small Bohr radius of the exciton. In ZnO, the Bohr radius is R_{Bohr} = 1.4 nm [32], which is the upper limit for a Li-Li dimer distance; more distant Li atoms cannot contribute simultaneously to the cooperative quantum cutting process.

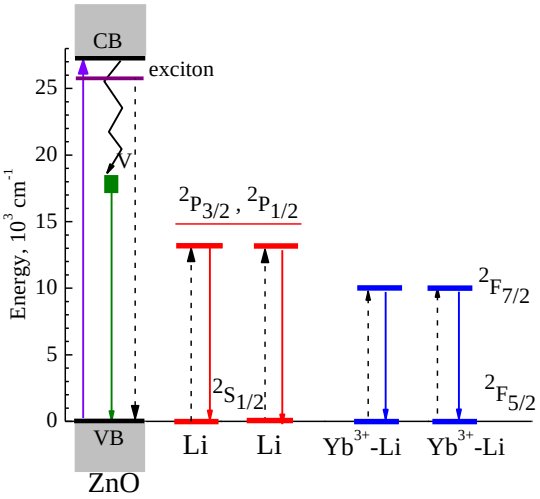

Fig. 6. Energy level diagram illustrating the energy transfer processes by quantum cutting from ZnO to Li-Li and to Yb^{3+}-Li nanoclusters. Excitation and emission transitions are shown by solid up-headed and down-headed arrows, respectively. A wavy black line shows de-excitation of electrons from the conduction band CB of ZnO to its intrinsic defect (oxygen vacancies) levels post-signed by the letter V, with subsequent emission of intrinsic green luminescence (green arrow). Thick red horizontal lines show energy levels of Li dimers/nanoclusters deduced from experimental data of Fig. 3c,d; the red down-headed arrows correspond to emission from Li-Li nanoclusters. Thin red horizontal line shows energy level of a single Li atom, which has the highest emission cross-section [29]. Blue horizontal lines show energy levels of Yb^{3+}-Li clusters and the blue arrows indicate an experimentally detected emission of Yb at about 1000 nm. Dashed black lines indicate an energy transfer processes by quantum cutting from the ZnO exciton to the Li-Li pairs/dimers and to the Yb^{3+}-Li pairs/dimers, respectively.

Very fortunately, the excited level of the Li-Li clusters locate equidistantly from the excited and the ground state of the exciton, which favors the quantum cutting mechanism for energy transfer from the exciton to the Li-Li dimers.

As concluded from the TEM EDX spectra in Fig. 2b, Yb^{3+} ions may also form dimer/nanoclusters states with Li ions, such as e.g. Yb^{3+}-Li. Indeed, the Yb emission spectrum about 1000 nm in our samples, Fig. 3d, differs from emission spectrum of Yb in ZnO host containing only Yb^{3+}, Fig. 3 in [11], indicating that Li ions slightly affect the electronic states of Yb^{3+} in the Yb^{3+}-Li nanoclusters. However, effect of Li on the emission band of Yb^{3+} is not large since Li is neutral.

The experimentally found excited levels of the Yb^{3+}-Li dimers and their ground states are shown for two neighboring dimers in Fig. 6 by blue horizontal lines and labeled schematically according to the energy levels of a single Yb^{3+}. These excited levels of Yb^{3+}-Li dimers are not so equidistant between the excited and the ground state of the exciton; this requires linear decay mechanism to be involved in the addition to the non-linear quantum cutting mechanism

#149477 - $15.00 USD Received 17 Jun 2011; revised 11 Jul 2011; accepted 19 Jul 2011; published 4 Aug 2011

in the case of energy transfer from ZnO to Yb dopants, in agreement with data of Fig. 5b and with Ref [12].

Finally, since the ZnO is a direct gap semiconductor it has a very high absorption cross-section in the range 300 to 420 nm which ensures that as thin as only several microns layer of ZnO:Li:Yb may work for down-conversion of solar spectrum for enhancement the response of Si solar cells. Therefore the ZnO:Li:Yb nanopowder dispersed in a polymer coating of several microns thickness may be employed in the down-conversion layers. Should the polymer be the photo-resist, the waveguides in the polymer layer may be structured for functionalizing the layer. As it is seen from Fig. 5, the doping level with Li and Yb at about 1 at.% ensures a co-operative energy transfer from ZnO to the dopants; this doping level agrees with typical values of doping level by Yb in other down-conversion systems, such as Tb^{3+}/Yb^{3+} system, e.g. in [33 and refs therein]. The high quantum efficiency of quantum cutting processes assures high energy transfer rate from ZnO to the dopants. ZnO may be modified by addition of other chemical elements [13–16], which could tailor its absorption edge to fit requirements of the particular solar cells.

5. Conclusion

We have heavily doped Li and Li-Yb into a nanocrystalline host of ZnO. The Li-Li and Yb^{3+}-Li dimer nanoclusters have been proposed to structure and to emit near infrared luminescence at 770 and 1000 nm, respectively. The emission has been argued to occur by a quantum cutting process from the exciton state of the ZnO. These phenomena will certainly have an implication for the down-conversion of the solar spectrum for enhanced Si solar cells.

Acknowledgement

We are grateful to the support from the FWO projects and from the Methusalem Funding of the Flemish Government. MVS acknowledges support from INPAC, KU Leuven.

#149477 - $15.00 USD Received 17 Jun 2011; revised 11 Jul 2011; accepted 19 Jul 2011; published 4 Aug 2011